Cell Reports
Article

Highly Canalized MinD Transfer and MinE Sequestration Explain the Origin of Robust MinCDE-Protein Dynamics

Jacob Halatek[1] and Erwin Frey[1,*]
[1]Arnold Sommerfeld Center for Theoretical Physics and Center for NanoScience, Department of Physics, Ludwig-Maximilians-Universität München, Theresienstraße 37, D-80333 München, Germany
*Correspondence: frey@lmu.de
DOI 10.1016/j.celrep.2012.04.005

SUMMARY

Min-protein oscillations in *Escherichia coli* are characterized by the remarkable robustness with which spatial patterns dynamically adapt to variations of cell geometry. Moreover, adaption, and therefore proper cell division, is independent of temperature. These observations raise fundamental questions about the mechanisms establishing robust Min oscillations, and about the role of spatial cues, as they are at odds with present models. Here, we introduce a robust model based on experimental data, consistently explaining the mechanisms underlying pole-to-pole, striped, and circular patterns, as well as the observed temperature dependence of the oscillation period. Contrary to prior conjectures, the model predicts that MinD and cardiolipin domains are not colocalized. The transient sequestration of MinE and highly canalized transfer of MinD between polar zones are the key mechanisms underlying oscillations. MinD channeling enhances midcell localization and facilitates stripe formation, revealing the potential optimization process from which robust Min-oscillations originally arose.

INTRODUCTION

Robust spatial patterning was crucial just from the beginning of cellular evolution and is key to the development of multicellular organisms. The oscillatory pole-to-pole dynamics of MinCDE proteins prevent improper cell divisions apart from midcell (Lutkenhaus, 2007; Raskin and de Boer, 1999). Due to its critical role for the cell cycle, a robust regulation of Min oscillations is of fundamental importance. As origin of robustness, an efficient mechanism, only depending on a few central molecular processes seems most likely. Indeed, experimental evidence supports a mechanism based on nonlinear reaction-diffusion dynamics. The Min proteins diffuse through the cytoplasm and the ATPase MinD attaches in its ATP-bound form to the cell membrane, where it recruits MinE, MinC, and MinD-ATP from the cytosol (Hu et al., 2002). MinC inhibits cell division, but plays no role in establishing oscillations (Lutkenhaus, 2007; Raskin and de Boer, 1999). MinE, which is present as a dimer (Shih et al., 2002; Ghasriani et al., 2010; Loose et al., 2011a; Park et al., 2011), hydrolyses MinD on the membrane and thereby initiates detachment. As consequence, pole-to-pole oscillations arise in wild-type cells, and striped oscillations in filamentous cells (Raskin and de Boer, 1999), revealing the presence of an intrinsic spatial wavelength. Experiments indicate that the temporal and spatial properties of patterns are established independently of each other, as temperature variations strongly affect the oscillation frequency, while leaving the spatial wavelength unchanged (Touhami et al., 2006). Thereby, proper cell division is ensured in a wide temperature range. In nearly spherical mutant cells one observes predominantly pole-to-pole oscillations along the major or an irregularly wandering axis, as well as circular waves on the membrane (Shih et al., 2005).

Numerous computational models have been proposed to elucidate Min-protein patterns (Kruse et al., 2007; Loose et al., 2011b). Most models are either based on recruitment of cytosolic proteins to the membrane (Huang et al., 2003; Fange and Elf, 2006; Loose et al., 2008; Arjunan and Tomita, 2010), differing mainly in their assumptions about the involved recruitment processes, or employ phenomenological nonlinearities (Meinhardt and de Boer, 2001; Howard et al., 2001; Meacci and Kruse, 2005) to reproduce the observed dynamics. The sheer number of conceptually different models accounting for specific observations underlines the generic nature of oscillatory dynamics in nonlinear systems, but leaves the actual underlying mechanisms ambiguous. The only known model that reproduces oscillatory patterns in cells with different shapes is based on recruitment (Fange and Elf, 2006). It was initially formulated in cylindrical geometry by Huang et al. (2003), and solely assumes experimentally verified or suggested reactions. However, in this model, striped oscillations only emerge for a nucleotide exchange rate below the experimentally determined lower bound (Meacci et al., 2006), and even then only for specific initial conditions that cannot account for the dynamic transition out of pole-to-pole oscillations (Touhami et al., 2006). Furthermore, the model could not provide the necessary robustness against parameter variations to account for temperature variations (Touhami et al., 2006; Di Ventura and Sourjik, 2011), therefore failing to explain proper cell divisions above room temperature. Finally, in contrast to pole-to-pole oscillations, patterns in spherical cells could only be explained by stochastic effects (Fange and Elf, 2006) or additionally included saturation terms (Huang and Wingreen, 2004).

The models' sensitivity to initial conditions and parameter variations raised doubts about the validity and completeness of recruitment-based models in general (Touhami et al., 2006). Moreover, striped patterns rather seem to arise in a small parameter set as a special case of the models possible dynamics, without being of any obvious biological relevance for the wild-type division cycle itself. One may therefore wonder why striped patterns arise at all. For the extension of present models, nucleation of MinD polymers at periodically distributed domains enriched with anionic phospholipids was suggested (Touhami et al., 2006). This would introduce a predetermined spatial template, which might stabilize Min-protein patterns by separating spatial organization from temporal dynamics. Indeed, some models assert Min oscillations to be induced by the nucleation of MinD filaments at the cell poles (Drew et al., 2005; Cytrynbaum and Marshall, 2007). This line of thought is based on the preference of MinD to bind in regions enriched with cardiolipin (Mileykovskaya et al., 2003; Mileykovskaya and Dowhan, 2009), an anionic phospholipid that clusters in domains of high negative membrane curvature (Renner and Weibel, 2011; Huang et al., 2006; Mukhopadhyay et al., 2008), like the cell poles. However, no colocalization of MinD stripes with cardiolipin domains has been reported so far, leaving the actual role of cardiolipin domains as spatial cue elusive.

As it is ubiquitous in many intracellular biochemical systems, the interactions between Min proteins are restricted to the lipid membrane, raising interesting questions about the role of cell geometry and spatial organization in spatiotemporal pattern formation. However, so far, a theoretical investigation of a model's dynamics is restricted to numerical simulations of a few single parameter configurations, leaving the overall parameter and geometry-dependent pattern-forming abilities largely elusive.

Here, we present a robust minimal model based on recruitment (Huang et al., 2003) that respects cellular geometry and allows broad parameter studies by linear stability analyses along with the incorporation of membrane diffusion. Employing a nonlinear reactive bulk-boundary coupling and distinct diffusion processes for the cytosol and the membrane, we reformulated the reaction-diffusion system in elliptical coordinates. The use of elliptical geometry was crucial, as it accounts for the various aspect ratios, and captures axial and circular patterns simultaneously, while still being amenable to linear stability analyses. In contrast to one-dimensional reductions (Loose et al., 2008), this ansatz allows the important distinction between circular waves and pole-to-pole oscillations.

The model reproduces all transitions between oscillatory patterns in wild-type, filamentous, and nearly spherical cells, as well as the temperature dependence of the temporal period. We find that the pattern-forming process neither adapts to spatial templates given by inhomogeneous MinD attachment, nor does it depend on variations of the hydrolysis rate or on initial conditions. In contrast, transitions between patterns are mediated by variations of the cell geometry alone. From the linear stability analysis and extensive numerical simulations, we find that the molecular key mechanisms behind Min oscillations are the transient sequestration of MinE proteins at the cell membrane, and a highly canalized transfer of MinD from old to new polar zones. We argue that robust formation and stabilization of patterns is completely defined by the system's nonlinear bulk-boundary couplings and geometric parameters and suggest that localized nucleation of MinD polymers is the secondary process guided by the spontaneous oscillations.

RESULTS

Bulk-Boundary Couplings in Cellular Geometry

To correctly account for membrane-cytosol exchange dynamics in cellular geometry, we attribute pattern formation to a reactive coupling of distinct species diffusing trough the spatially extended cytosol and the cellular membrane. Previous comparable analytical approaches were restricted to circular geometries and linear bulk-boundary couplings, with spatial patterning relying on bulk degradation (Levine and Rappel, 2005). Here, we advance these methods to elliptical geometries and nonlinear reactive boundary conditions, which generally account for possible multimolecular reactions between cytosolic and membrane-bound species. Moreover, we adapted the system parameters to meet recent experiments (Meacci et al., 2006; Loose et al., 2011a), and disregarded cooperative recruitment of cytosolic MinD (Huang et al., 2003) or MinE (Loose et al., 2008) by MinDE complexes, as both processes lack experimental verification (Loose et al., 2011a). The resulting reaction scheme is based on four molecular processes: attachment, detachment, recruitment, and nucleotide exchange. It is described in Figure 1A. Total particle numbers are conserved, as synthesis and degradation of proteins does not affect the oscillation in vivo (Raskin and de Boer, 1999). We chose orthogonal elliptical coordinates, given by the normal μ and tangential ν components at the boundary, see Figure S1. The ensuing set of reaction-diffusion equations reads:

$$\partial_t u_{DT} = D_D \nabla^2 u_{DT} + \lambda u_{DD} \tag{1}$$

$$\partial_t u_{DD} = D_D \nabla^2 u_{DD} - \lambda u_{DD} \tag{2}$$

$$\partial_t u_E = D_E \nabla^2 u_E \tag{3}$$

$$\partial_t u_d = D_d \nabla_\nu^2 u_d + u_{DT}(k_D + k_{dD} u_d) - k_{dE} u_E u_d \tag{4}$$

$$\partial_t u_{de} = D_{de} \nabla_\nu^2 u_{de} + k_{dE} u_E u_d - k_{de} u_{de}, \tag{5}$$

with nonlinear reactive boundary conditions stating that the reactions equal the flux onto (−) and off (+) the membrane

$$D_D \nabla_\mu u_{DT}\big|_{\mu=\mu_0} = -u_{DT}(k_D + k_{dD} u_d) \tag{6}$$

$$D_D \nabla_\mu u_{DD}\big|_{\mu=\mu_0} = k_{de} u_{de} \tag{7}$$

$$D_E \nabla_\mu u_E\big|_{\mu=\mu_0} = k_{de} u_{de} - k_{dE} u_E u_d. \tag{8}$$

Here, u_{DT}, u_{DD}, and u_E denote the bulk concentrations of MinD-ATP, MinD-ADP, and MinE, respectively, and u_d, u_{de} the

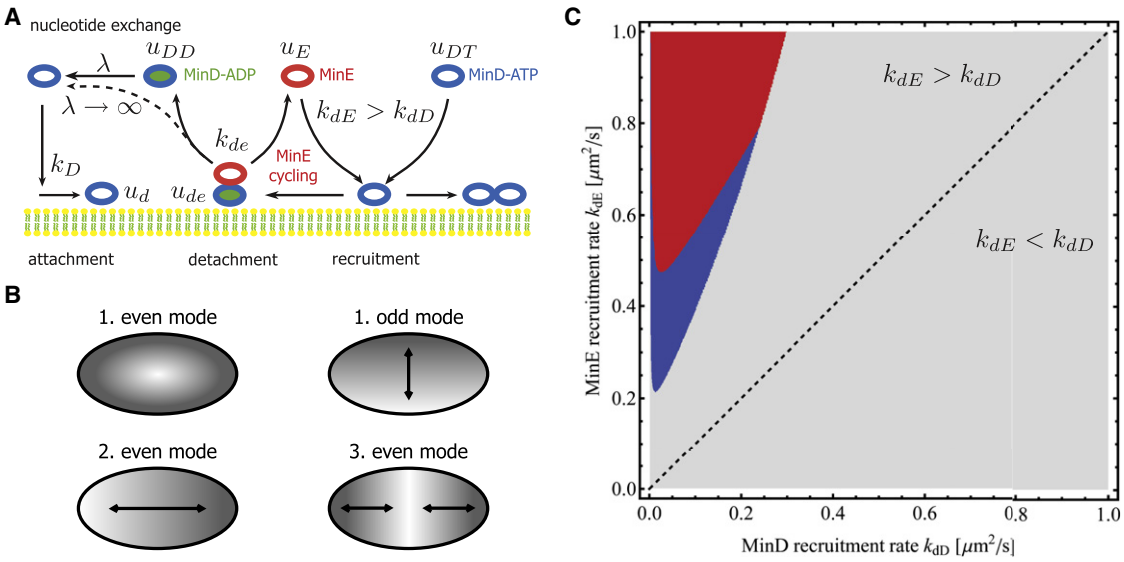

Figure 1. Minimal Model Dynamics and Dynamical Instabilities

(A) Cytosolic MinD-ATP attaches to the membrane with a rate k_D, where it recruits further MinD-ATP and MinE from the cytosol with rates k_{dD} and k_{dE}, respectively. Recruitment of MinE leads to the formation of MinDE complexes, which disintegrate to cytosolic MinD-ADP and MinE with the temperature-dependent hydrolysis rate $k_{de} \propto \exp(-E_A/RT)$. Finally, MinD-ADP exchanges nucleotides with rate λ. The scheme highlights the possibility of local MinE cycling, given a sufficiently high density of membrane bound MinD.

(B) Schematic illustration of even and odd modes in elliptical geometry.

(C) Phase portrait for both recruitment processes illustrates the condition on the recruitment rates (Equation 9) for dynamical instabilities with $k_{de} = 0.65s^{-1}$. In the gray domain, the system is stable below cell lengths of $2\mu m$. The colored region shows where only even modes (blue) or even and odd modes (red) are unstable at cell lengths below $2.8\mu m$. Numerical simulations determined that only pole-to-pole oscillations are selected in the red domain.

membrane concentrations of MinD and MinDE complexes. The limit of instantaneous nucleotide exchange is obtained by replacing both cytosolic MinD species with $u_D = u_{DT} + u_{DD}$. We will also study the implication of this limiting case, as it was assumed in some previous models (Kruse et al., 2007; Loose et al., 2008). In elliptical geometry, patterns along the major or minor axis are expressed by even and odd modes, respectively, see Figure 1B. The even modes correspond to pole-to-pole and striped oscillations. Which modes grow or oscillate can be determined by linear stability analysis, see Supplemental Information for the technical details.

Conditions on the System Parameters for Spatial Pattern Formation

The model parameters are as far as they are available fixed by experimental data: We use the diffusion constants (Meacci et al., 2006; Loose et al., 2011a) $D_D = 16\mu m^2/s, D_E = 10\mu m^2/s$, $D_d = D_{de} = 0.013\mu m^2/s$, and a nucleotide exchange rate $\lambda = 6s^{-1}$ to meet the lower bound (Meacci et al., 2006) of $3s^{-1}$. Regarding particle numbers, we assume a linear scaling with cell size that corresponds to a total number of $N_D = 2000$ MinD monomers and $N_E = 700$ MinE dimers in a wild-type elliptical cell of $5\mu m$ length and $1\mu m$ width (Shih et al., 2002; Unai et al., 2009) which yields a MinD/MinE ratio of 2.86. We note that all discussed observations can be reproduced equally well for MinD/MinE ratios of 1.43, where MinD and MinE are both considered as dimers, see Supplemental Information for discussion and Figure S2.

Lacking further in vivo measurements, the remaining parameters were adjusted to reproduce all experimentally observed oscillatory patterns (Raskin and de Boer, 1999; Shih et al., 2005; Touhami et al., 2006). Based on our analytical approach in elliptical geometry, we were able to identify pattern-forming instabilities through linear stability analysis already on timescales below 0.1s. This is by order of magnitudes faster than what can be achieved by full simulation runs, which usually take tens of minutes for single parameter configurations. This technical progress allows us to investigate large parameter spaces and thereby make general assessment about a model's validity. By sampling parameter space for pole-to-pole oscillations at cell lengths about $2\mu m$, we were able to determine that, for spatial patterns to emerge in general, MinE needs to be recruited faster to the membrane than MinD (Figure 1C), while being lower in total particle number:

$$k_{dD} < k_{dE}, \tag{9}$$

$$N_E < N_D. \tag{10}$$

While the specific ratio of recruitment rates and particle numbers up to which oscillations persist depends on all system parameters, the above conditions were always fulfilled. The implications on the specific mechanism of pattern formation will be discussed in the next section. The model parameters were further refined by accounting for temperature variations and testing the model for striped and circular patterns with

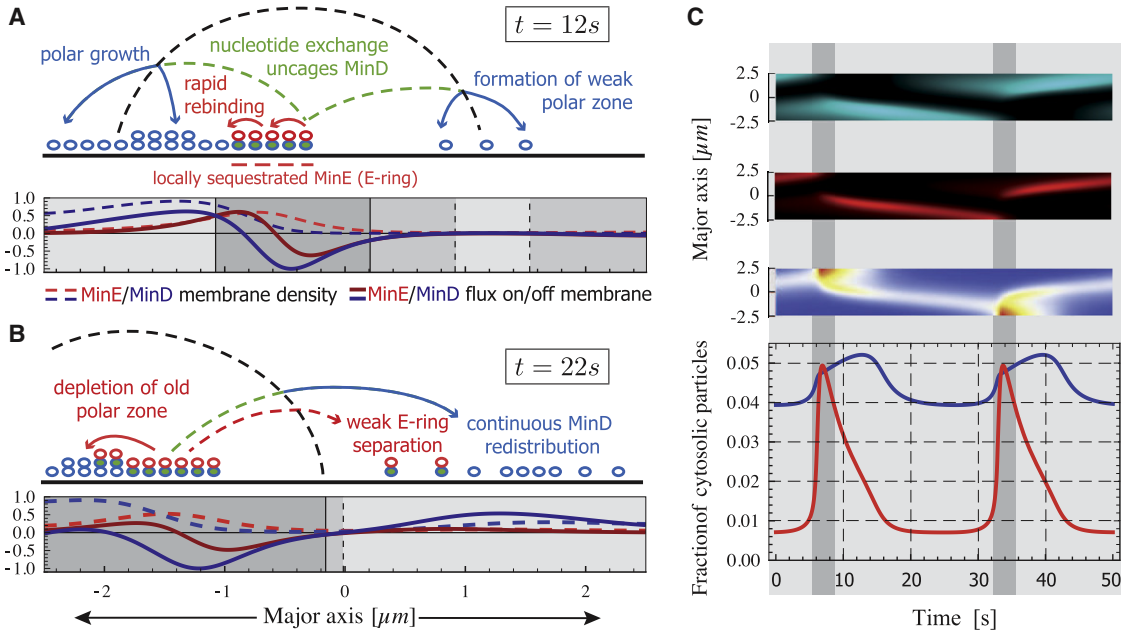

Figure 2. Key Mechanisms Underlying Min Oscillations

(A) Locally sequestrated MinE constitutes the MinE ring, which moves toward the left pole through local cycling. Detaching MinD rebinds predominately at the left pole and initiates a weak polar zone at the right end. The delayed reattachment due to nucleotide exchange is indicated by dashed lines. The numerical data below correspond to the time step $t = 12s$ in Figure 2C (densities are scaled by a factor $2.5\times10^{-3}\mu m^{-1}$, fluxes by a factor $1.8\times10^{-2}\mu m^{-1}s^{-1}$). The accentuation shows regions of dominant MinD attachment (light) or MinE attachment (dark). These adjoin to regions (gray) where MinD accumulation is suppressed due to dominant MinE detachment.

(B) MinE depletes the old polar zone of MinD, until only MinDE complexes are left, then reassembles at the rim of the new polar zone, formed by redistributed MinD. The numerical data correspond to the time step $t = 22s$ in Figure 2C (densities are scaled by a factor $2.6\times10^{-3}\mu m^{-1}$, fluxes by a factor $2.2\times10^{-2}\mu m^{-1}s^{-1}$).

(C) Top: kymographs at $T = 22.5^{\circ}C$: membrane densities of MinD+MinDE (turquoise), MinDE (red), and the fraction MinDE/MinD in logarithmic color scale. Bottom: Fractions of total cytosolic particles, MinD (blue) and MinE (red). Accentuated regimens correspond to transient sequestration (light) and rapid relocalization (dark) of MinE.

cf. Movie S1.

numerical simulations. Regarding the temperature dependence, we assume an Arrhenius law for the hydrolysis rate k_{de}, with an activation energy $E_A = 16.7kcal/mol$ and normalization $k_{de}(20^{\circ}C) = 0.4s^{-1}$. The remaining parameters are

$$k_D = 0.1\mu ms^{-1}, k_{dD} = 0.108\mu m^2 s^{-1}, k_{dE} = 0.435\mu m^2 s^{-1}. \quad (11)$$

These values will serve as reference in further discussions of the model's parameter dependencies.

Min Oscillations Are Caused by Transient Sequestration of MinE

How do patterns emerge in the minimal model defined by the above reaction-diffusion Equations 1–8? The conservation of particle numbers ascribes formation and growth of any spatial pattern to a global redistribution of membrane-bound proteins through cytosolic diffusion. MinD is driven off the membrane upon binding MinE through stimulation of ATPase activity. Thereby MinE counteracts the accumulation of MinD at the membrane and drives the displacement of MinD. Polar zones can grow if the local MinE density is sufficiently low, and MinD particles are gradually transferred from MinDE domains to the polar zone. Figure 2 illustrates how the formation and separation of MinD and MinDE domains follows from the conditions on particle numbers and recruitment rates, Equations 9 and 10, stated above. The higher particle number of MinD (Equation 10) enables complete sequestration of MinE in membrane-bound MinDE complexes, still leaving a fraction of MinD available to initiate a new polar zone. Given a sufficiently high MinD membrane concentration and MinE recruitment rate k_{dE}, detaching MinE rebinds immediately, forming the prominent MinE ring (Lutkenhaus, 2007; Raskin and de Boer, 1997; Derr et al., 2009), see Figures 2A and 2C and Movie S1. Continuous MinE cycling locally depletes the membrane from MinD, leading to a slow movement of the MinE ring along the gradient of membrane bound MinD, whereupon a fraction of detaching MinD initiates a weak polar zone in the opposite cell half, see Figure 2A. The new polar zone grows due to steady redistribution of MinD, while most MinE remains sequestrated in the old polar zone (Figure 2B) until the remaining MinD are converted into MinDE complexes (Figures 2B and 2C). Once this state is reached, the Min proteins rapidly detach, diffuse through the cytosol and rapidly reattach at the new polar zone (cf. Movie S1), leaving behind a region of high MinDE/MinD ratio, where immediate reformation of polar zones is inhibited, cf. Figure 2C. Due to the faster recruitment of MinE (Equation 9) the MinE ring

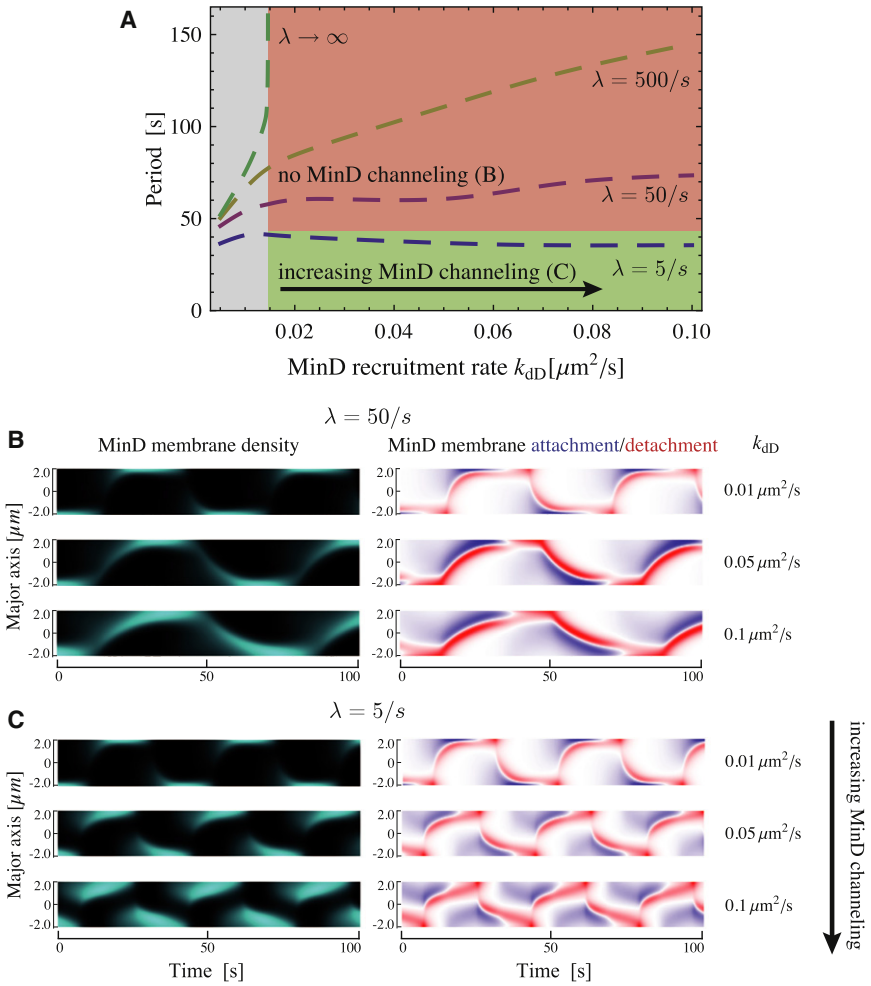

Figure 3. Canalized MinD Transfer and Regulation of Spatial MinD Reattachment by MinD Recruitment

(A) Temporal period as function of MinD recruitment k_{dD} and nucleotide exchange λ in cells of $4\mu m$ length at $T = 25^\circ C$. With instantaneous nucleotide exchange, oscillations only exist at low MinD recruitment rates (gray). Beyond this threshold, the nucleotide exchange and recruitment rates become control parameters for the spatial distribution of MinD reattachment. At high but finite nucleotide exchange rates the oscillation period increases with the MinD recruitment rate as MinD reassembles in front of the polar zone, cf. Figure 3B below. At low nucleotide exchange rates the oscillation period decreases with MinD recruitment as the pole-to-pole particle transfer becomes canalized between both cell halves, cf. Figure 3C below.

(B) Kymographs for $\lambda = 50s^{-1}$ showing the total MinD membrane density $u_d + u_{de}$ and MinD flux $D_D \nabla_\mu (u_{DT} + u_{DD})|_{\mu = \mu_0}$ on (blue) and off (red) the membrane for stepwise increasing MinD recruitment rates. At higher MinD recruitment rates MinD is not depleted but reflected at the cell poles. In this case MinD reattaches in front of a moving MinD wave.

(C) Analogous kymographs for $\lambda = 5s^{-1}$. Here, MinD reaccumulates at the opposite cell pole. Increasing MinD recruitment accelerates the growth of new polar zones toward midcell and synchronizes depletion and formation of polar zones at opposite cell ends by canalizing the MinD flux from old to new polar zones.

reassembles at the rim of the new polar zone, which provides the crucial separation of MinD and MinDE maxima. Otherwise, MinE would diffuse into the polar zone and accumulate at the MinD maximum, deplete it, and suppress further formation of MinD domains. Moreover, we observed that the MinE recruitment rate k_{dE} regulates the width of the MinE ring and the timescale of polar zone recovery after disintegration. For higher MinE recruitment rates MinE rings narrow and the recovery timescale increases as MinD reaccumulation is stronger suppressed by sequestrated MinE. The sequestration of MinE is transient, and the system oscillatory, if detaching MinD gradually leaks from polar zones. But how is MinD leakage established and regulated?

Cytosolic MinD Transfer Is Regulated by MinD Recruitment

It was argued that oscillations are sustained by the delayed MinD-ATP recovery (Huang et al., 2003), while the exchange rate λ itself has small impact on the oscillatory dynamics (Touhami et al., 2006). Indeed, our analysis confirms that the oscillation period depends rather weakly on the exchange rate λ (Figure 3A). However, while the system stays oscillatory at high MinD recruitment rates k_{dD} even for unrealistically fast but finite exchange rates, it becomes stationary polarized in the limiting case of an instantaneous exchange, if the MinD recruitment rate exceeds a certain low threshold, cf. Figure 3A. This threshold increases with the MinD attachment rate k_D and decreases with cell length. These results can be understood by considering the spatiotemporal regulation of MinD reattachment by MinD recruitment and recovery.

The MinD recruitment rate k_{dD} defines the "stickiness" of polar zones for cytosolic MinD-ATP. In contrast, a finite nucleotide exchange rate λ uncages MinD from polar zones as MinD only binds to the membrane in its active ATP form. The faster the nucleotide exchange, and the stronger the recruitment, the less particles leak from polar zones. This is evident from the slowing down of the oscillation with increasing nucleotide exchange and MinD recruitment rates, depicted in Figure 3A, and agrees with previous findings (Huang et al., 2003; Touhami et al., 2006). With fast nucleotide exchange, MinD does not reaccumulate at the bare membrane before the old pole is depleted, whereas the MinD recruitment rate mainly regulates the reaccumulation position (Figure 3B). On the other hand, for nucleotide exchange rates close to the experimentally determined lower bound of $3s^{-1}$, reaccumulation always starts in the opposite

cell half, and the recruitment of MinD regulates how fast the new polar zone grows toward the old one (Figure 3C). Now, the period peaks at a low MinD recruitment rate $k_{dD} = 0.015 \mu m^2/s$ and decreases with MinD recruitment from 41.2*s* to 35.6 s at the global minimum around $k_{dD} = 0.1 \mu m^2/s$, cf. Figure 3A. This minimum marks parameter configurations where the redistribution of MinD from old to new polar zone is highly canalized, i.e., the total MinD flux is directed toward the opposite cell half immediately after the polar zones starts to shrink (Figure 3C). Thereby, growth and depletion of polar zones become synchronized. This leads to the characteristic triangular shape observed in MinD kymographs (Loose et al., 2011b), where new polar zones start growing toward midcell while old polar zones shrink toward the cell pole, cf. Figure 3C. As rebinding of MinD to the old polar zone is inhibited by delayed ATP recovery, and the growth of new polar zones is promoted by strong MinD recruitment, the oscillation period decreases as a function of the MinD recruitment rate due to a faster redistribution of MinD. Recall that the recovery of polar zones is suppressed by MinE recruitment, which highlights the interdependence of both recruitment processes. Although the system's dynamics is diffusive, which, per se, is an undirected process, the coupling of bulk diffusion and nucleotide exchange with nonlinear recruitment to the membrane enables regulation of the pole-to-pole particle transfer. While the uncaging effect of nucleotide exchange has been noticed previously (Huang et al., 2003), the role of MinD recruitment has been unknown, so far. Neglecting explicit nucleotide exchange as in earlier models (Loose et al., 2008) restricts the parameter space to low MinD recruitment rates. In this case, new polar zones do not grow until old polar zones are disassembled, cf. Figures 3B and 3C. The following sections will reveal that canalizing MinD transfer enhances the biological function of Min oscillations and enables robust stripe formation in the first place.

Canalized MinD Transfer Improves the System's Efficiency and Midcell Localization Accuracy

The functional purpose of Min oscillations is the inhibition of Z-ring assembly apart from midcell by ongoing consumption of ATP. In this regard it is favorable to establish a high and permanent MinD membrane occupancy at the cell poles, ideally with the smallest number of attachment events during each oscillation cycle. For the localization of Z-ring assembly to be most precise, the mean MinD density should show a pronounced minimum at midcell with a high contrast to the cell poles. As shown in Figure 4A, the mean MinD density is always minimal at midcell, but its particular shape strongly depends on the MinD recruitment rate k_{dD}. Since the typical environment of *Escherichia coli* is the lower intestine of warm-blooded organisms, oscillations are considered at body temperature. The cell length is set to $5 \mu m$.

To measure the optimality of Min oscillations, we introduce two quantities. First, and most important, we ask for the accuracy of midcell localization. This depends on the accentuation of midcell in the MinD density profile. We distinguish between the width and the depth of the mean MinD density minimum at midcell, cf. Figure 4B. If the ratio between width and depth of the minimum is smallest, midcell is most distinctly accentuated. We find a well-defined and unique optimal value for the MinD recruitment rate k_{dD} (Figure 4C), which, in addition, is very close to the fitted value (cf. Equation 11). The optimum coincides with the value where the MinD transfer is highly canalized. Increasing the MinD recruitment rate accelerates the growth of polar zones toward midcell, such that the mean density decreases at the cell tips, and increases at midcell, cf. Figure 4A. If the MinD recruitment rate is too low, i.e., much lower than the MinE recruitment rate, recovery of polar zones is suppressed by the predominant rebinding of cytosolic MinE, such that polar zones form at late stages of the oscillation cycle and therefore are constrained to the cell tips, cf. Figure 3C.

In a previous approach (Kerr et al., 2006), the precision of midcell localization, depending on the MinD/MinE density ratio, has been investigated for the model by Huang et al. (2003). An acceptable precision could only be obtained at unrealistically high MinD/MinE ratios. Comparing the deterministic data with our results, we find that precision is substantially increased in the present model, even at the protein density ratios determined by experiments.

The second measure describes the efficiency with which MinD occupies the membrane, hence relates the mean membrane occupancy with the ATP consumption per oscillation cycle. While reducing ATP consumption alone might be rather subordinate, a higher MinD membrane density directly affects the probability of recruiting the division inhibitor MinC to the membrane. Again, we find an optimal value for the MinD recruitment rate k_{dD} that corresponds to highly canalized MinD transfer (Figure 4D). Lower k_{dD} values reduce the mean MinD membrane density, while higher k_{dD} values increase the number of (re-)attachment events during polar zone disassembly but do not increase the mean MinD membrane density much more due to saturation effects.

From the evolutionary perspective, adjusting the pole-to-pole transfer of particles is beneficial and distinguishes favorable configurations out of the large parameter space. A refinement of MinD recruitment increases the accuracy of midcell localization and optimizes the system's ability to occupy the membrane with MinD. Since Min oscillations are highly robust against variations of the recruitment rates (cf. Figure 1C), it seems plausible that the system was optimized through gradual refinement of the recruitment process.

MinE Sequestration Explains the Persistent Binding of MinE Observed In Vitro

Recent experiments revealed a persistent binding of MinE at the rear of MinD domains in vitro (Loose et al., 2011a), even without direct MinE membrane interactions. With the transient sequestration of MinE, our model provides an explanation for this observation: The lower particle number of MinE enables sequestration, while fast MinE recruitment confines sequestration spatially, thereby inducing growth of MinD domains. Subsequently, continual leakage of MinD from the polar zones renders sequestration transient, hence the system oscillatory. In particular, the sharp decrease in protein densities at the end of the oscillation cycle is the result of spontaneously suspended sequestration (Figure 2C). Albeit an extension by explicit MinE membrane interactions was suggested (Arjunan and Tomita, 2010; Hsieh et al., 2010; Park et al., 2011), additional sequestration of MinE by

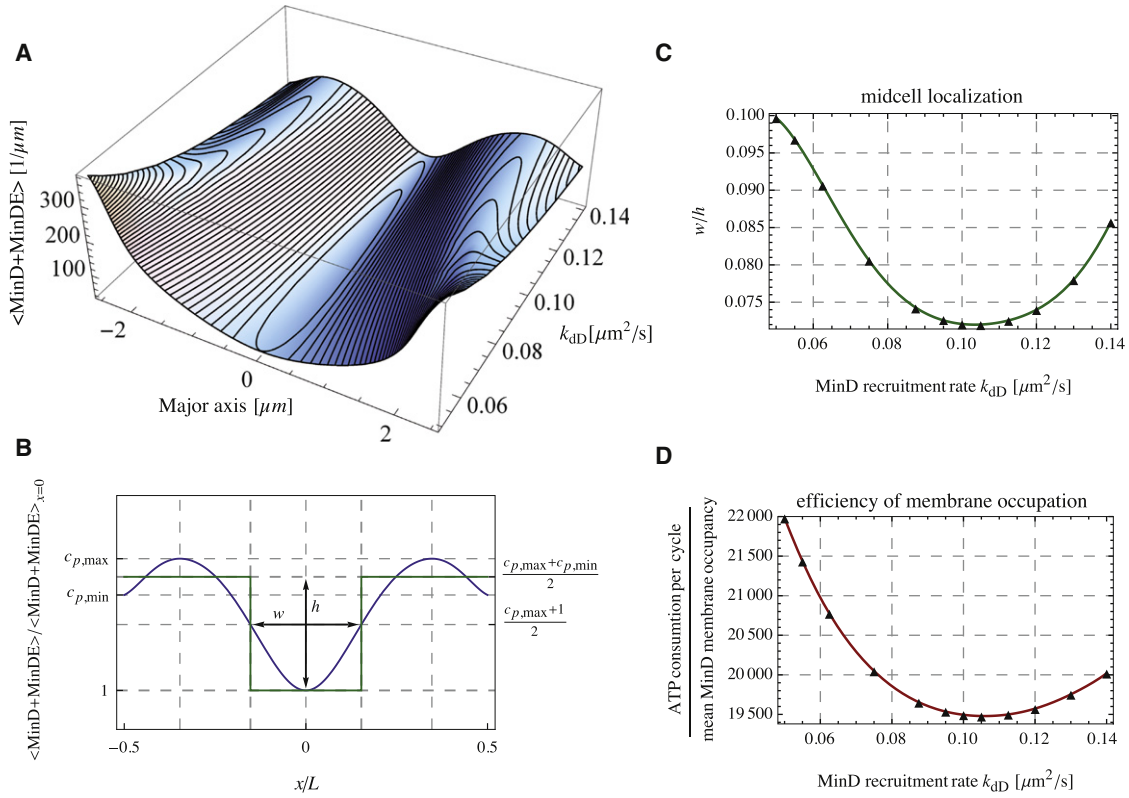

Figure 4. Optimization of Pole-to-Pole Oscillations by Canalized MinD Transfer at T = 37.5°C

(A) Mean MinD membrane density during one oscillation cycle as function of the MinD recruitment rate k_{dD}. With increasing MinD recruitment, polar zones grow dynamically toward midcell, reflected in a decreased distance between the maxima in the density profile.

(B) Characterization of the mean MinD membrane density by the width w and depth h of the MinD density minimum at midcell. The axial coordinate x is rescaled by the cell length L. The density is rescaled by its value at x = 0.

(C) Optimal midcell localization, defined as the minimum of w / h as a function of the MinD recruitment rate. Optimum at $k_{dD} = 0.103 \mu m^2/s$. The solid line shows the interpolation of the numerical data (triangles).

(D) Efficiency of pole-to-pole oscillations, defined as the ratio of ATP consumption per cycle and the mean MinD membrane occupancy as a function of the MinD recruitment rate. Optimum at $k_{dD} = 0.106 \mu m^2/s$. The solid line shows the interpolation of the numerical data (triangles).

transient membrane bonds would merely amplify the argued mechanism, while introducing additional experimentally undetermined parameters. However, by implementing the recently proposed "tarzan of the jungle"-mechanism (Park et al., 2011) in our model, we found that delayed MinE detachment from the membrane can weaken the condition on the particle numbers, Equation 10, while additional cycling of MinE on the membrane by rapid recombination with MinD cannot replace the condition on the recruitment rates, Equation 9. As a consequence, cytosolic cycling remains the key process, showing that the minimal model dynamics comprise a suitable skeleton model where future extensions can be build upon. In this respect it would be highly beneficial to obtain the exact ratio of MinD and MinE densities in vivo up to which regular Min oscillations persist, as well as the quantitative aspects of MinE interactions on and with the membrane.

Striped Patterns Dynamically Emerge Out of Pole-to-Pole Oscillations

Next we demonstrate that the set of four molecular processes (Figure 1A) suffices to reproduce all oscillatory patterns, see Figure 5 and the Supplemental Information for the corresponding movies. First, we consider the transition of pole-to-pole to striped oscillations. As observed in vivo (Raskin and de Boer, 1999, 1997), if the cell length exceeds a certain threshold an additional polar zone with an accompanying MinE ring emerges out of pole-to-pole oscillations such that MinD oscillates between both cell poles and midcell. The transition from pole-to-pole to stripe oscillations occurs dynamically as the cell grows, cf. (Loose et al., 2011b). Hence, for the emergence of stable stripe states, one important precondition is that pole-to-pole oscillations become unstable first. Otherwise, either no transition would occur at all, or one could expect stochastic switching between both patterns. However, the transition to stripes is very robust and even independent of system temperature (Touhami et al., 2006). These observations are at odds with previous theoretical studies that found that the formation of stripes depends on initial conditions (Touhami et al., 2006), or that stochastic fluctuations lead to switching between traveling waves and striped oscillations (Tostevin and Howard, 2006). Therefore, we chose a pole-to-pole wave solution peaking in one cell half as initial condition, and determined the rate

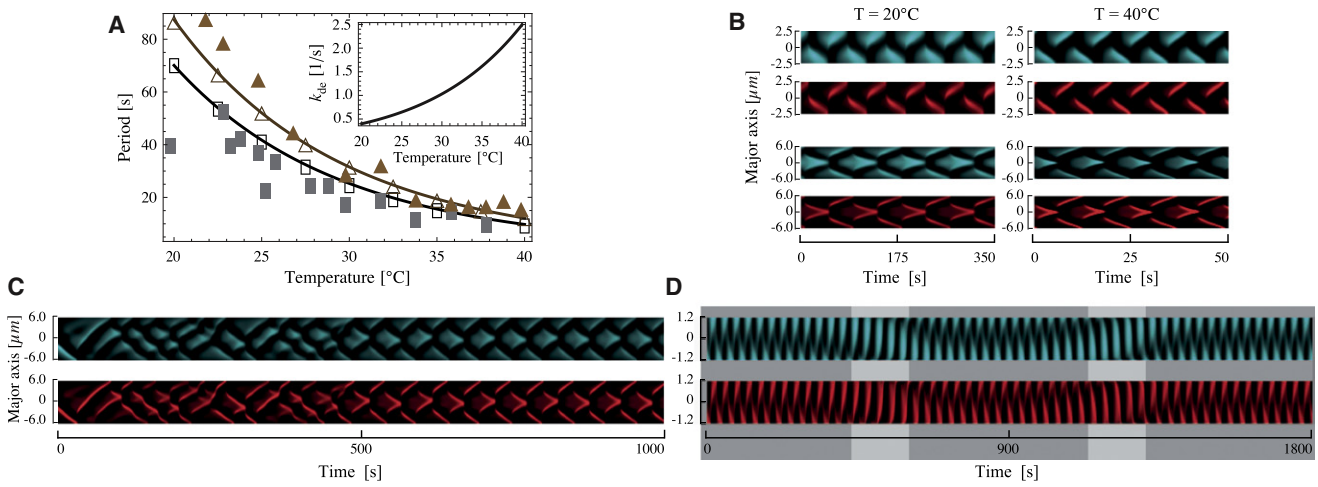

Figure 5. The Temperature Dependence and the Dynamic Adaptation of Spatial Patterns to Cell Geometry

(A) Temperature-dependent periods of pole-to-pole (open rectangles) and striped (open triangles) oscillations with their according Arrhenius fits ($E_A = 18 kcal/mol$), see Supplemental Information for discussion. Cell lengths are $5\mu m$ and $12\mu m$, respectively. Filled rectangles and triangles show experimental data by Touhami et al. (2006) for cells of $4\mu m - 5\mu m$ and tens of μm length, respectively. Inset shows temperature-dependent hydrolysis rate.

(B) Kymographs of membrane densities MinD+MinDE (turquoise) and MinDE (red) for pole-to-pole (top) and striped oscillations (bottom). cf. Movies S2, S3, S4, and S5.

(C) Example of stripe formation out of traveling waves. cf. Movie S6.

(D) Kymographs of membrane densities in the upper cell half for nearly spherical cells ($2.4\mu m$ length, $2.2\mu m$ width) show switching between predominant pole-to-pole oscillations (dark) and circular waves (light). cf. Movie S7.

See also Figure S2.

constants (Equation 11) that yield transitions into stable stripes. This choice of initial conditions was crucial, as the choices made in previous studies (Fange and Elf, 2006) proved insufficient for parameter refinement, see Supplemental Information. We confirm that stable stripes are absent in a reduced one-dimensional geometry with reflecting boundaries (Huang et al., 2003). However, we did find stable striped oscillations in the analogous two-dimensional rectangular geometry with reflecting polar caps, indicating that the spatial separation of bulk and membrane is essential for stripe formation. In terms of the scheme in Figures 2A and 2B, increasing the cell length promotes the simultaneous formation and depletion of two MinD domains through continuous redistribution of MinD and MinE, leading to colliding unidirectional traveling waves and ultimately the striped pattern, see Figure 5C and Movie S6. We found that stable stripes emerge out of pole-to-pole waves, only if weak polar zones are enhanced early on by sufficiently strong MinD recruitment, $k_{dD} > 0.1 \mu m^2/s$. Hence, stripe formation and the optimization of the wild-type oscillation cycle are based on the same mechanism. Since striped patterns are irrelevant for the wild-type division cycle per se, and are only supported in a small subset of the oscillatory parameter regimen (cf. Figure 1C), they seem to result from an evolutionary optimization of wild-type oscillations.

An Arrhenius Law for the Hydrolysis Rate Accounts for Temperature Variations

The reproducibility of temperature dependencies poses a further critical test on the model's robustness. Figure 5A shows the period of pole-to-pole and striped oscillations as a function of temperature, implemented through the hydrolysis rate $k_{de} \propto \exp(-E_A/RT)$, with the activation energy $E_A = 16.7 kcal/mol$, the gas constant R, and the absolute temperature T. In agreement with experiments (Touhami et al., 2006), the period-temperature relation is given by an Arrhenius law. Over the complete temperature range, and for all initial conditions, the final patterns stayed qualitatively unchanged, see Figure 5B and Movies S2, S3, S4, and S5. This result highlights the importance of a systematic parameter refinement, as even recent expositions report a loss of oscillations with varying hydrolysis rate (Di Ventura and Sourjik, 2011). In contrast, our model reveals a strong robustness over a large range of hydrolysis rates. Increasing the temperature leads to faster local cycling of Min proteins between membrane and cytosol. With each cycle, a fraction of MinD leaks from the polar zone. As a consequence, the temporal period decreases due to a faster redistribution of particles, but the spatial wavelength remains unaffected, as it does not depend on the detachment process. However, oscillations can be lost with increasing hydrolysis rate k_{de} if either attachment or recruitment of MinD is chosen too low. In these cases, an accumulation of MinD at the membrane is impeded by rapid detachment. This provides a possible explanation for the parameter sensitivity observed in previous accounts (Touhami et al., 2006; Di Ventura and Sourjik, 2011). Note that the polar zones and MinE rings narrow with increasing temperature (cf. Figure 5B). This can be explained by the decreased residence time of membrane-bound proteins, which reduces the distance proteins diffuse on the membrane before detachment. Accordingly, we find that the narrowing effect vanishes if membrane diffusion is either turned off, or increased sufficiently

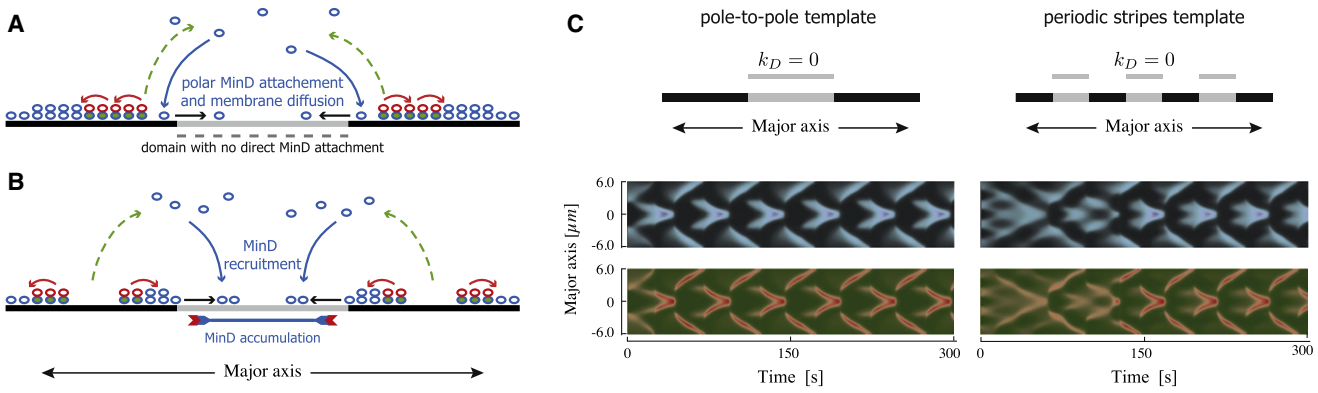

Figure 6. Effect of Spatial Cues on Spatiotemporal Pattern Formation

(A) MinD attachment is restricted to the cell poles. Following polar MinD attachment, MinD diffuses toward midcell.

(B) Even without direct MinD attachment, a MinD zone forms at midcell due to slow membrane diffusion and fast MinD recruitment from the cytosol.

(C) Kymographs of Min oscillations in filamentous cells with spatially restricted MinD attachment, MinD (blue), MinE (red/green). Left: restricting MinD attachment to the cell poles does not jeopardize stripe formation. Right: adding further attachment domains corresponding to the next striped pattern does not promote additional stripe formation.

See also Figure S2.

along with temperature. Since all diffusion constants depend on temperature, the narrowing of polar zones and MinE rings might be too weak to notice experimentally, or even completely compensated by faster diffusion. Regarding possible temperature dependencies of the remaining parameters the system remains robust: To account for temperature increase ($k_{de} = 2.5 s^{-1}$), all other system parameters, i.e., diffusion constants and kinetic rates, can be increased jointly up to a factor of about eight without changing the spatial wavelength. If the upscaling of the diffusion constants is limited to a factor two, the kinetic rates can be increased jointly up to threefold. Due to this robustness, we did not include explicit temperature dependencies for the remaining parameters.

Striped Patterns Do Not Adapt to Cardiolipin Domains

The results above demonstrate that spatial cues are not necessary to ensure robust patterns. However, as MinD preferentially binds to anionic phospholipids like cardiolipin found at the cell poles (Mileykovskaya et al., 2003; Mileykovskaya and Dowhan, 2009), we asked if oscillatory patterns adapt to spatial templates. We considered two different templates for filamentous cells by restricting MinD attachment to predefined parts of the membrane, see Figure 6C. First, a template for the pole-to-pole oscillation, where direct MinD attachment is restricted to both cell poles, and second, a periodic template corresponding to the next stripe state given by four separate attachment domains. In both cases, and for various initial conditions, the patterns finally evolved into the original striped oscillation, i.e., no adaption could be observed, see Figure 6C. We find that slow diffusion of membrane-bound MinD, which is followed by fast recruitment, suffices to promote the formation of robust MinD domains even without foregoing MinD attachment, cf. Figures 6A and 6B. This observation demonstrates that the initial position of MinD attachment does not categorically determine the final position of MinD stripes. In contrast to recruitment, the MinD attachment process does not amplify membrane bound patterns, but merely increases the MinD membrane density throughout the cell. Accordingly, we find for the model with spatially homogeneous MinD attachment, that varying the attachment rate k_D rather leads to the loss of instability than to a qualitative change of the spatial pattern.

So, which processes do regulate the characteristic wavelength? From the discussion of the channeling mechanism, we know that the interplay between MinD recruitment and finite nucleotide exchange affects the growth rate of new MinD domains toward the old ones. On the other hand, the MinE recruitment rate k_{dE} defines a minimal distance between MinD stripes, as it determines the width of the MinE ring, and thereby the zone where the accumulation of MinD is suppressed, cf. Figures 2A and 2B. Of course, the distance between detachment and re-recruitment also depends on the bulk diffusion coefficients. In contrast, being pronounced membrane-bound structures, MinE rings and MinD stripes widen independently of the recruitment rates with increasing membrane diffusion. In summary, it is the interplay of all processes, and not a specific one, that defines the characteristic wavelength: from the kinetic rates it is the recruitment processes that affect the pattern's spatial properties most, but, in general, varying these rates alone does not suffice to drive the system into a regular higher order striped state without increasing cell length.

Geometry Selects Patterns in Nearly Spherical Cells

Patterns in nearly spherical cells result from the additional destabilization of odd modes, see Figure 1B. For instance, in cells of $2.4 \mu m$ length and $2.2 \mu m$ width we observed predominant pole-to-pole oscillations along the major axis over a period of about 535 s that fade to circular waves and oscillations along a rotating axis for about 175 s, until pole-to-pole oscillations are reestablished again, see Figure 5D and Movie S7. Additionally, as a random switching of the traveling direction was observed for circular waves in vivo (Shih et al., 2005), it occurs between consecutive phases of circular waves in the deterministic model.

After the division of nearly spherical cells, one observes a shift of the oscillation axis by 90° toward the cell's new long axis (Shih et al., 2005). We employed a deformed mesh technique to increase the cell's width dynamically beyond its length, and likewise observed a shift toward the major axis, see Movie S8. Taken together, our findings indicate that this variety of patterns is primarily caused by weak aberrations from spherical symmetry, and not by stochastic effects or unstable higher order modes, as presumed previously (Fange and Elf, 2006; Huang and Wingreen, 2004).

DISCUSSION

Our analysis identifies transient MinE sequestration to be the key mechanism behind Min oscillations. Sequestration of MinE is based on a lower particle number of MinE or, alternatively, on direct interactions between MinE and the lipid membrane. We find that the faster recruitment of MinE confines sequestration to the rim of polar zones and continual leakage of MinD from old to new polar zones renders sequestration transient. The cellular geometry imposes a nonlinear bulk-boundary coupling, which is key for the selection and stabilization of spatial patterns.

How do MinD filaments, cardiolipin domains, and irregular patterns fit in this picture? Several models accounting for Min-protein filaments assert the nucleation of MinD polymers to be mediated, and thereby localized, by cardiolipin domains at the cell poles (Drew et al., 2005; Cytrynbaum and Marshall, 2007). Consequently, all patterns in filamentous cells ought to be determined by a dynamic periodic template of cardiolipin domains with an intrinsic spatial wavelength. However, neither a presence of periodic templates, nor a colocalization of MinD and cardiolipin domains has been reported in filamentous cells so far. Moreover, as cardiolipin adapts to membrane curvature, so should MinD, but, based on the limited available data, bending filamentous cells does not seem to affect the spatial MinD patterns (cf. e.g., Raskin and de Boer, 1999; Touhami et al., 2006). The mechanism presented in this paper is independent of, and, in fact, robust against spatial cues. This suggests a different origin for MinD nucleation: MinD filaments have been reported in two different setups. In vivo, helical MinD filaments only appear along with Min oscillations (Shih et al., 2003). In particular, MinD settles in a homogeneous membrane-bound state without any additional ordered structure, if the cell is lacking MinE, and therefore oscillations. This observation immediately follows from our model, as membrane diffusion removes any potential inhomogeneities caused by spatially restricted MinD attachment. Helical MinD filaments were also observed at high MinD concentrations in vitro (Hu et al., 2002). In presence of ATP and phospholipid vesicles, MinD assembles in helical structures. Taking both observations together, nucleation of MinD filaments could be promoted at high local MinD densities in vivo. In this case, the nonlinear dynamics described by our model provide the primary mechanism, necessary to induce MinD nucleation at the polar zones, suggesting that MinD polymerization is the consequence and not the origin of spontaneous pattern formation. This scenario resembles the directed assembly of actin cables guided by polar caps of the GTPase Cdc42 in yeast (Wedlich-Soldner et al., 2003).

Irregular patterns, like stochastic pole-to-pole switching in short cells (Fischer-Friedrich et al., 2010), or aberrant oscillations in cells mutant for MinE (Hsieh et al., 2010), imply the loss of robustness. In our model, robustness and oscillatory patterns share the same origin. Formation and growth of polar zones and MinE rings is impelled by strong recruitment of MinD and MinE and only constrained by the finite number of available particles. The character of Min oscillations is highly nonlinear, with the cell length acting as natural parameter driving the system from dynamical equilibrium toward highly stable limit cycles corresponding to the individual patterns. Therefore, irregular patterns can only arise in regimens where the system dynamics are moved close to primal bifurcation points. In these regimens close to threshold the system is highly susceptible to fluctuations, such that stochastic dynamics, spatial irregularities, and additional molecular processes that were irrelevant for the regular pattern-forming process might play a crucial role. For instance, stochastic pole-to-pole switching were only observed in short cells with lengths below $2.7\mu m$ (Fischer-Friedrich et al., 2010), which is close to the onset of dynamical instability in our model. An investigation of these phenomena, however, is only possible in a stochastic model.

Another example for irregularities is given by the appearance of aberrant oscillations in cell mutant for MinE (MinE C1) (Hsieh et al., 2010). As these mutant MinE lack the ability to bind to the lipid membrane, direct MinE membrane interactions were suggested as an important process for robust Min oscillations. However, the C1 mutant also shows a reduced interaction strength with MinD. Reducing the MinE recruitment rate in our model drives the system toward dynamical equilibrium, suggesting that the reduced MinE-MinD interaction and not the loss of MinE-membrane interactions might have disturbed the oscillatory dynamics in the first place. This example emphasizes that conclusions drawn from irregular dynamics do not necessarily hold for regular Min oscillations, as critical regimens might be dominated by mechanisms not included in the minimal model due to their weak influence on the regular dynamics. Accordingly, further experiments should be performed in close contact with theoretical modeling. In particular, experiments with the MinE-C1 mutant could validate the sequestration mechanism, as the model predicts that patterns vanish when the MinE concentration approaches the MinD concentration.

Beyond that, a multitude of predictions immediately follows from our results on MinD channeling. For instance, striped patterns should vanish, and accurate cell divisions be compromised, if the MinD recruitment rate could be significantly reduced. Moreover, patterns should vanish, if the MinE recruitment process is weakened severalfold.

The model also predicts an Arrhenius law for the hydrolysis rate with an activation energy about $16.7 kcal/mol$. Quantitative knowledge about the temperature dependencies of the various reactions involved in Min-protein dynamics would improve further theoretical investigations substantially.

Reaching for a complete and coherent account to the Min system as a whole, the next step is to apply the model to in vitro dynamics (Loose et al., 2008, 2011a) and to verify the sequestration mechanism experimentally. As a preliminary result, we note that the current model sustains bands of synchronous traveling

waves as observed in vitro (Loose et al., 2008, 2011a), even without extending the reaction scheme (Figure 1A) by the suggested nonlinear detachment (Loose et al., 2011a) of Min proteins or cooperative MinE recruitment (Loose et al., 2008).

On a broader perspective, the presented theoretical formalism enables the investigation of protein dynamics in vivo and in vitro with explicit account for the underlying system geometries and nonlinear bulk-boundary couplings. Examples are intracellular polarization mechanisms driven by reaction-diffusion processes, e.g., in *Caenorhabditis elegans* (Goehring et al., 2011) or *Saccharomyces cerevisiae* (Johnson, 1999).

EXPERIMENTAL PROCEDURES

Numerical Simulations and Initial Conditions

All time-dependent computations were performed with finite element methods on a triangular mesh using Comsol Multiphysics 3.5a. As initial conditions, linear profiles along the cell's long axis with varying slopes and small random fluctuations at each mesh site were chosen. In these cases all particles were initially located in the bulk. The traveling wave initial condition used in simulations with filamentous cells was obtained by choosing a low MinD recruitment rate about $k_{dD} = 0.03 \mu m^2/s$ and picking the traveling wave solution at a time step where the total MinD concentration was maximal in one cell half.

SUPPLEMENTAL INFORMATION

Supplemental Information includes Extended Results, Extended Experimental Procedures, two figures, and eight movies and can be found with this article online at doi:10.1016/j.celrep.2012.04.005.

LICENSING INFORMATION

ACKNOWLEDGMENTS

The authors thank Andrew Rutenberg and Manfred Jericho for kindly providing their data (Touhami et al., 2006) and Ulrich Gerland for critical reading of the manuscript. This project has been financially supported by the German Excellence Initiative via the program "Nanosystems Initiative Munich" (NIM).

Received: July 23, 2011
Revised: January 26, 2012
Accepted: April 18, 2012
Published online: June 7, 2012

REFERENCES

Arjunan, S.N., and Tomita, M. (2010). A new multicompartmental reaction-diffusion modeling method links transient membrane attachment of E. coli MinE to E-ring formation. Syst. Synth. Biol. *4*, 35–53.

Cytrynbaum, E.N., and Marshall, B.D.L. (2007). A multistranded polymer model explains MinDE dynamics in E. coli cell division. Biophys. J. *93*, 1134–1150.

Derr, J., Hopper, J.T., Sain, A., and Rutenberg, A.D. (2009). Self-organization of the MinE protein ring in subcellular Min oscillations. Phys. Rev. E Stat. Nonlin. Soft Matter Phys. *80*, 011922.

Di Ventura, B., and Sourjik, V. (2011). Self-organized partitioning of dynamically localized proteins in bacterial cell division. Mol. Syst. Biol. *7*, 457.

Drew, D.A., Osborn, M.J., and Rothfield, L.I. (2005). A polymerization-depolymerization model that accurately generates the self-sustained oscillatory system involved in bacterial division site placement. Proc. Natl. Acad. Sci. USA *102*, 6114–6118.

Fange, D., and Elf, J. (2006). Noise-induced Min phenotypes in E. coli. PLoS Comput. Biol. *2*, e80.

Fischer-Friedrich, E., Meacci, G., Lutkenhaus, J., Chaté, H., and Kruse, K. (2010). Intra- and intercellular fluctuations in Min-protein dynamics decrease with cell length. Proc. Natl. Acad. Sci. USA *107*, 6134–6139.

Ghasriani, H., Ducat, T., Hart, C.T., Hafizi, F., Chang, N., Al-Baldawi, A., Ayed, S.H., Lundström, P., Dillon, J.-A.R., and Goto, N.K. (2010). Appropriation of the MinD protein-interaction motif by the dimeric interface of the bacterial cell division regulator MinE. Proc. Natl. Acad. Sci. USA *107*, 18416–18421.

Goehring, N.W., Trong, P.K., Bois, J.S., Chowdhury, D., Nicola, E.M., Hyman, A.A., and Grill, S.W. (2011). Polarization of PAR proteins by advective triggering of a pattern-forming system. Science *334*, 1137–1141.

Howard, M., Rutenberg, A.D., and de Vet, S. (2001). Dynamic compartmentalization of bacteria: accurate division in E. coli. Phys. Rev. Lett. *87*, 278102.

Hsieh, C.-W., Lin, T.-Y., Lai, H.-M., Lin, C.-C., Hsieh, T.-S., and Shih, Y.-L. (2010). Direct MinE-membrane interaction contributes to the proper localization of MinDE in E. coli. Mol. Microbiol. *75*, 499–512.

Hu, Z., Gogol, E.P., and Lutkenhaus, J. (2002). Dynamic assembly of MinD on phospholipid vesicles regulated by ATP and MinE. Proc. Natl. Acad. Sci. USA *99*, 6761–6766.

Huang, K.C., and Wingreen, N.S. (2004). Min-protein oscillations in round bacteria. Phys. Biol. *1*, 229–235.

Huang, K.C., Meir, Y., and Wingreen, N.S. (2003). Dynamic structures in Escherichia coli: spontaneous formation of MinE rings and MinD polar zones. Proc. Natl. Acad. Sci. USA *100*, 12724–12728.

Huang, K.C., Mukhopadhyay, R., and Wingreen, N.S. (2006). A curvature-mediated mechanism for localization of lipids to bacterial poles. PLoS Comput. Biol. *2*, e151.

Johnson, D.I. (1999). Cdc42: An essential Rho-type GTPase controlling eukaryotic cell polarity. Microbiol. Mol. Biol. Rev. *63*, 54–105.

Kerr, R.A., Levine, H., Sejnowski, T.J., and Rappel, W.-J. (2006). Division accuracy in a stochastic model of Min oscillations in Escherichia coli. Proc. Natl. Acad. Sci. USA *103*, 347–352.

Kruse, K., Howard, M., and Margolin, W. (2007). An experimentalist's guide to computational modelling of the Min system. Mol. Microbiol. *63*, 1279–1284.

Levine, H., and Rappel, W.J. (2005). Membrane-bound Turing patterns. Phys. Rev. E Stat. Nonlin. Soft Matter Phys. *72*, 061912.

Loose, M., Fischer-Friedrich, E., Ries, J., Kruse, K., and Schwille, P. (2008). Spatial regulators for bacterial cell division self-organize into surface waves in vitro. Science *320*, 789–792.

Loose, M., Fischer-Friedrich, E., Herold, C., Kruse, K., and Schwille, P. (2011a). Min protein patterns emerge from rapid rebinding and membrane interaction of MinE. Nat. Struct. Mol. Biol. *18*, 577–583.

Loose, M., Kruse, K., and Schwille, P. (2011b). Protein self-organization: lessons from the min system. Annu. Rev. Biophys. *40*, 315–336.

Lutkenhaus, J. (2007). Assembly dynamics of the bacterial MinCDE system and spatial regulation of the Z ring. Annu. Rev. Biochem. *76*, 539–562.

Meacci, G., and Kruse, K. (2005). Min-oscillations in Escherichia coli induced by interactions of membrane-bound proteins. Phys. Biol. *2*, 89–97.

Meacci, G., Ries, J., Fischer-Friedrich, E., Kahya, N., Schwille, P., and Kruse, K. (2006). Mobility of Min-proteins in Escherichia coli measured by fluorescence correlation spectroscopy. Phys. Biol. *3*, 255–263.

Meinhardt, H., and de Boer, P.A. (2001). Pattern formation in Escherichia coli: a model for the pole-to-pole oscillations of Min proteins and the localization of the division site. Proc. Natl. Acad. Sci. USA *98*, 14202–14207.

Mileykovskaya, E., and Dowhan, W. (2009). Cardiolipin membrane domains in prokaryotes and eukaryotes. Biochim. Biophys. Acta *1788*, 2084–2091.

Mileykovskaya, E., Fishov, I., Fu, X., Corbin, B.D., Margolin, W., and Dowhan, W. (2003). Effects of phospholipid composition on MinD-membrane interactions in vitro and in vivo. J. Biol. Chem. *278*, 22193–22198.

Mukhopadhyay, R., Huang, K.C., and Wingreen, N.S. (2008). Lipid localization in bacterial cells through curvature-mediated microphase separation. Biophys. J. *95*, 1034–1049.

Park, K.-T., Wu, W., Battaile, K.P., Lovell, S., Holyoak, T., and Lutkenhaus, J. (2011). The Min oscillator uses MinD-dependent conformational changes in MinE to spatially regulate cytokinesis. Cell *146*, 396–407.

Raskin, D.M., and de Boer, P.A. (1997). The MinE ring: an FtsZ-independent cell structure required for selection of the correct division site in E. coli. Cell *91*, 685–694.

Raskin, D.M., and de Boer, P.A. (1999). Rapid pole-to-pole oscillation of a protein required for directing division to the middle of Escherichia coli. Proc. Natl. Acad. Sci. USA *96*, 4971–4976.

Renner, L.D., and Weibel, D.B. (2011). Cardiolipin microdomains localize to negatively curved regions of Escherichia coli membranes. Proc. Natl. Acad. Sci. USA *108*, 6264–6269.

Shih, Y.L., Fu, X., King, G.F., Le, T., and Rothfield, L. (2002). Division site placement in E.coli: mutations that prevent formation of the MinE ring lead to loss of the normal midcell arrest of growth of polar MinD membrane domains. EMBO J. *21*, 3347–3357.

Shih, Y.L., Le, T., and Rothfield, L. (2003). Division site selection in Escherichia coli involves dynamic redistribution of Min proteins within coiled structures that extend between the two cell poles. Proc. Natl. Acad. Sci. USA *100*, 7865–7870.

Shih, Y.L., Kawagishi, I., and Rothfield, L. (2005). The MreB and Min cytoskeletal-like systems play independent roles in prokaryotic polar differentiation. Mol. Microbiol. *58*, 917–928.

Tostevin, F., and Howard, M. (2006). A stochastic model of Min oscillations in Escherichia coli and Min protein segregation during cell division. Phys. Biol. *3*, 1–12.

Touhami, A., Jericho, M., and Rutenberg, A.D. (2006). Temperature dependence of MinD oscillation in Escherichia coli: running hot and fast. J. Bacteriol. *188*, 7661–7667.

Unai, S., Kanthang, P., Junthon, U., Ngamsaad, W., Triampo, W., Modchang, C., and Krittanai, C. (2009). Quantitative analysis of time-series fluorescence microscopy using a spot tracking method: application to Min protein dynamics. Biologia *64*, 27–42.

Wedlich-Soldner, R., Altschuler, S., Wu, L., and Li, R. (2003). Spontaneous cell polarization through actomyosin-based delivery of the Cdc42 GTPase. Science *299*, 1231–1235.